



Detached-Eddy Simulations Past a Circular Cylinder

ANDREI TRAVIN, MICHAEL SHUR, MICHAEL STRELETS and
PHILIPPE SPALART

*Federal Scientific Center “Applied Chemistry”, St. Petersburg 197198, Russia and Boeing
Commercial Airplanes, P.O. Box 3707, Seattle, WA 98124, U.S.A.*

Abstract. The flow is calculated with laminar separation (LS) at Reynolds numbers 50,000 and 140,000, and with turbulent separation (TS) at 140,000 and 3×10^6 . The TS cases are effectively tripped, but compared with untripped experiments at very high Reynolds numbers. The finest grid has about 18,000 points in each of 56 grid planes spanwise; the resolution is far removed from Direct Numerical Simulations, and the turbulence model controls the separation if turbulent. The agreement is quite good for drag, shedding frequency, pressure, and skin friction. However the comparison is obscured by large modulations of the vortex shedding and drag which are very similar to those seen in experiments but also, curiously, durably different between cases especially of the LS type. The longest simulations reach only about 50 shedding cycles. Disagreement with experimental Reynolds stresses reaches about 30%, and the length of the recirculation bubble is about double that measured. The discrepancies are discussed, as are the effects of grid refinement, Reynolds number, and a turbulence-model curvature correction. The finest grid does not give the very best agreement with experiment. The results add to the validation base of the Detached-Eddy Simulation (DES) technique for smooth-surface separation. Unsteady Reynolds-averaged simulations are much less accurate than DES for LS cases, but very close for TS cases. Cases with a more intricate relationship between transition and separation are left for future study.

Key words: separation, simulation, cylinder, turbulence.

1. Motivation

The DES treatment of turbulence, described in the appendix, is aimed at the prediction of separated flows at unlimited Reynolds numbers and at a manageable cost. The claim is that it soundly combines fine-tuned Reynolds-Averaged Navier–Stokes (RANS) technology in the boundary layers, and the simple power of Large-Eddy Simulation (LES) in the separated regions [26]. In the RANS regions, the turbulence model has full control over the solution, but it is used within a plausible envelope. In the LES region, little control is left to the model, the larger eddies are resolved, and grid refinement directly expands the range of scales in the solution, and therefore the accuracy of the nonlinear interactions available to the largest eddies [24]. The computing-cost outcome is favorable enough that a challenging separated flow, namely an airfoil at high angles of attack and fairly high Reynolds

numbers, was treated quite successfully on personal computers [23]. This is the case although DES is a three-dimensional, time-dependent approach.

The sphere and the circular cylinder are obvious test cases for an approach with claims over separated flows. Constantinescu and Squires [5] present a DES study of the sphere, which is roughly as successful as the present one but does not include TS cases (also, RANS is more accurate in their flow than here). Our work on a thin airfoil [23] exercised both the RANS and the LES capability of DES, but not truly in the same solution. A pure RANS method would give the same solution as DES at low angles of attack, the flow being attached. A pure LES method could give fair results at high angles of attack, the major features of the flow having little sensitivity to the boundary-layer turbulence (which an LES of the whole domain could not resolve with present computers). After massive separation the smaller eddies which depend on the subgrid-scale (SGS) and molecular viscosities have little control, and even a Reynolds number of 250 preserves much of the physical character of the flow, such as three-dimensionality and shedding modulations [14]. Our airfoil paper also lacked extensive grid-refinement studies, and we include some here.

A point of great interest in DES is the “grey area” between RANS and LES regions. At separation, the shear layer has no “LES content” (i.e., 3D unsteady eddies the size of the boundary-layer thickness). DES is most plausible if a rapid new instability, of larger scale, overwhelms the turbulence inherited from the boundary layer if any. This is more likely when separation is from a sharp edge or at least a thin one, as on the airfoil. The cylinder is less forgiving, and a better test case for “grey-area failures”.

Finally, the cylinder is known for its drag crisis, which reflects the great differences in separation between laminar and turbulent boundary layers. Cases with turbulent separation are out of reach of whole-domain LES. The challenges in DES are not trivial. Laminar-separation (LS) cases are not challenging in terms of separation prediction proper; however, the model needs to be dormant in the laminar region, and arise in a spontaneous manner after separation, which can be delicate. Shur et al. [22] introduced the trip-less (TL) approach. The inflow eddy viscosity is zero, or at least much smaller than the molecular viscosity. The front part of the boundary layer then also has zero eddy viscosity. The recirculation region has non-zero eddy viscosity, and these finite values propagate upstream to the separation region. There, eddy viscosity diffuses into the separating shear layer. The vorticity in that layer causes rapid production of eddy viscosity, which then enters the recirculation region. The result is a self-sustaining eddy-viscosity field. It occurs only if non-zero values were placed in the initial condition, but the details of the initial field are erased. The mature solution depends only on the turbulence model, and no transition information (location, extent) is provided by the user. We have used the TL approach for the cylinder flow in 2D unsteady RANS (URANS) [22] but with coarser grids than here, and for a separation bubble in 2D RANS [28].

Turbulent-separation (TS) cases give the model control over separation, which stresses its accuracy as in traditional RANS tests. Therefore, a campaign including both LS and TS cases presents a few possibilities for failures. TS cases use either one of the standard methods to obtain eddy viscosity in the attached boundary layer with the S-A model. The first method is to use the trip term [25], with the trip placed on the front of the cylinder, say at $\theta = 60^\circ$. This is a source term added locally to the eddy-viscosity transport equation. The second, which we used, is to set the inflow value of eddy viscosity $\tilde{\nu}$ to about 5 times the molecular viscosity. The result is that as soon as fluid enters the boundary layer, the production term is active and the eddy viscosity rapidly comes into equilibrium with the velocity field, with turbulent profiles. In all cases, the Turbulence Index i_t indicates the state of the boundary layer [25].

To summarize, the conditions which distinguish LS and TS cases are the following. LS cases have $\tilde{\nu} = 0$ at the inflow boundary, but $\tilde{\nu} \neq 0$ in the initial condition. TS cases have $\tilde{\nu} \neq 0$ at the inflow boundary. Non-zero inflow or initial values for $\tilde{\nu}$ are of the order of 5 times the molecular viscosity ν .

All studies of flows in 2D geometries, whether experimental or numerical, face the challenge of understanding and conveying the dependence on boundary conditions in the third direction. We have no doubt that 3D simulations are necessary for “2D” bluff-body flows [9, 12, 14, 18]. These bring in arbitrariness in the type of spanwise conditions and the domain size Λ_z . We have used periodicity and $\Lambda_z = 2 \times D$, where D is the cylinder diameter, and did not conduct extensive sensitivity tests. Other bluff-body studies have used lengths up to $2\pi \times D$, showing very acceptable differences; recent cylinder work used $1 \times D$ to $\pi \times D$ [3, 8].

Note how different the criterion used for setting Λ_z for bluff-body flows has been from that used in DNS of channels or boundary layers [10]. There, a negligible correlation at a half-period in the spanwise direction is the goal. In bluff-body flows, a strong correlation of the shedding over the period is deemed acceptable, and two-point correlations rarely presented [29, 30]. This is true in simulations, and also in experiments: for instance Schewe presented the lift signal from a balance for a model with a length equal to $10 \times D$, thus recognizing coherence over at least that distance [21]. A numerical domain-size study aimed at bringing the two-point correlation to small values appears hopeless. Szepessy’s experimental results [30] suggest a bare minimum of $15 \times D$. The best we can do is to demonstrate that our results have a weak enough sensitivity to significant changes in the domain size, preferably a doubling.

DNS, LES and DES in nontrivial geometries make grid design a broad challenge. Systematic tests may give the most reliable answers, but are extremely time-consuming. Also, measures of success are ambiguous, especially when the numerous sources of error compensate. It would be naïve to adjust an aspect of the method just to obtain a “perfect” drag coefficient C_d , for instance. In a recent LES study it was found “astonishing” that grid refinement did not always improve results, where “improve” meant “bring closer to experiments” [3]. An excellent point.

Therefore, we view grid changes more as tests of soundness and sensitivity than as a search for perfection. We apply simple rules for grid design, such as seeking cubic grid cells in the LES region (the SGS eddies being statistically isotropic in the first approximation) and describing each grid with only a representative grid spacing Δ . We may find later that the rules were sub-optimal, but we observe that refinement is more convincing if the grid is refined in all directions simultaneously, instead of one at a time.

Based on these observations we believe that the cylinder taken over the LS and TS régimes represents a substantial test case for DES, giving the opportunity to show that it is very competitive with both RANS and LES. Success would suggest that hybrid methods, while unattractive “engineering” tools in the eyes of some, will be the basis of turbulence prediction for a large class of flows.

2. Simulations

2.1. NUMERICAL CHARACTERISTICS

The cases are split into series with laminar separation, LS1 to LS9, and turbulent separation, TS1 to TS12, see Tables I and II. The full matrix of cases has not been filled; in particular, only one fine-grid case is available, LS3. Further fine-grid LS cases will be valuable, but they take months, and will be launched only after deeper study of the optimal grid and time step. Fine-grid TS runs do not appear necessary in view of the very weak grid dependence from coarse to medium. LSE and TSE denote the experimental references [1, 4, 15, 19–21]. LSJ is the LES of Jordan and Ragab [8] at $Re = 5,600$, and the Reynolds-number difference must be kept in mind. LSB is the LES of Breuer [3] at 140,000; we selected the more representative of his cases (A1, A2, B1, B2), which still leaves a fair amount of scatter (also note that the time-step comparison is misleading since our code has about 20 subiterations per full time step). LSA and TSA are 2D unsteady Reynolds-averaged simulations, and L2D and T2D are 2D DES (such simulations are not natural, and only run as thought experiments).

Within the LS and the TS series, cases differ by their Reynolds number, grid spacing, and model (some include the rotation/curvature term [27], as indicated in the “RC” column). The Reynolds-number dependence should be weak once the separation type is specified. We are aiming at the simpler flow types, denoted as TrSL3 (transition in the shear layers, upper Reynolds-number range) and T (fully turbulent) by Zdravkovich [31]. The grid spacing Δ in the table denotes the “target Δ ” and is measured near $(x, y) = (0.75, 0.5)$, where there is high activity and the solution is clearly of LES type. Recall that the local Δ in DES is the largest of the spacings in all directions, here r , θ , and z . The 3D grids are balanced, in the sense that Δ_z is close to the target Δ , thus resulting in the cubic grid cells mentioned in Section 1. The Δ ratio between successive grids is about $\sqrt{2}$, and all terms are treated to at least second-order accuracy. Typical values for the CFL number are 0.5 in the wake, and 2 outside the boundary layer at the crest of the cylinder.

Table I. Summary of cases.

Run	Re	Grid	Δ	Δt	RC	t	C_d	$-C_{pb}$
LS1	5×10^4	118, 105, 30	0.068	0.05	n	200	1.05	0.98
LS2	5×10^4	150, 109, 42	0.048	0.05	n	127	1.26	1.28
LS3	5×10^4	210, 135, 57	0.034	0.035	n	186	1.32	1.39
LS4	5×10^4	118, 105, 30	0.068	0.05	y	104	1.17	1.15
LS5	5×10^4	150, 109, 42	0.048	0.05	y	99	1.14	1.08
LS7	1.4×10^5	118, 109, 30	0.068	0.05	n	200	0.87	0.81
LS8	1.4×10^5	150, 109, 42	0.048	0.05	n	280	1.08	1.04
LSJ	5.6×10^3	241, 241, 32	–	–	–	30	1.01	1.02
LSB	1.4×10^5	325, 325, 64	–	0.0002	–	65/170	1.22/1.45	1.4/1.8
LSA	5×10^4	210, 135	0.034	0.035	n	–	1.8	2.23
L2D	5×10^4	210, 135	0.034	0.035	n	–	1.77	2.05
LSE	$\approx 10^5$	–	–	–	–	–	1.15/1.25	1.2
TS1	1.4×10^5	118, 105, 30	0.068	0.05	n	200	0.57	0.65
TS2	1.4×10^5	150, 109, 42	0.048	0.05	n	158	0.59	0.67
TS4	1.4×10^5	118, 105, 30	0.068	0.05	y	88	0.64	0.70
TS5	1.4×10^5	150, 109, 42	0.048	0.05	y	73	0.65	0.70
TS7	3×10^6	118, 115, 30	0.068	0.05	n	50	0.41	0.53
TS10	3×10^6	118, 115, 30	0.068	0.05	y	24	0.51	0.64
TSA	1.4×10^5	150, 109	0.048	0.035	n	–	0.56	0.59
T2D	1.4×10^5	150, 109	0.048	0.035	n	–	0.83	1.18
TSE	$\approx 5 \times 10^6$	–	–	–	–	–	0.5/0.8	0.5/0.9

The numerical method uses a fifth-order upwind scheme, and an implicit three-layer second-order-accurate scheme for time integration, with artificial compressibility. Constantinescu and Squires [5] also adopted a fifth-order upwind scheme after experimenting. The use of upwind, monotone, or otherwise dissipative discretizations in DNS, LES or DES is controversial. We would prefer centered schemes of course, and used one for LES of homogeneous turbulence [23]. However, for the cylinder, just as for the airfoil, this scheme does not work due to a lack of stability resulting in spatial oscillations of the solution, first of all, in the RANS regions. The causes are well known. They are: high values of the cell Reynolds number (even based on eddy viscosity), dispersion, especially at angles to the grid lines, non-uniform grid spacing and coefficients, nonlinearity. We are developing an algorithm that is centered in LES regions, and upwind-biased in the RANS and irrotational regions.

We consider that numerical issues will permanently require attention. However, a statement such as “upwind schemes are unacceptable for LES” cannot be correct.

Table II. Summary of cases.

Run	C'_l	St	θ_{sep}	L_r	L_{vv}	$\overline{u'u'}_{\text{max}}$	$\overline{u'v'}_{\text{max}}$	$\overline{v'v'}_{\text{max}}$
LS1	0.21	0.22	78°	1.3	1.5	0.20	0.13	0.46
LS2	0.48	0.21	80°	0.8	0.9	0.34	0.17	0.66
LS3	0.66	0.20	96°	0.8	0.9	0.37	0.15	0.62
LS4	0.40	0.19	80°	0.9	1.1	0.26	0.14	0.56
LS5	0.27	0.20	78°	1.1	1.3	0.25	0.14	0.53
LS7	0.10	0.23	78°	1.5	1.7	0.15	0.11	0.38
LS8	0.29	0.21	77°	1.1	1.2	0.25	0.14	0.50
LSJ	0.12	0.21	87°	–	1.6	0.20	0.12	0.42
LSB	–	0.20/0.22	95°	0.4/0.6	1.2	–	0.13/0.15	0.8/1
LSA	1.47	0.22	90°	–	–	–	–	–
L2D	1.39	0.14/0.20	–	–	–	–	–	–
LSE	0.24/0.6	0.18/0.21	80°	0.44/0.75	1.1	0.25	0.12	0.44
TS1	0.08	0.30	99°	1.1	1.3	0.12	0.09	0.32
TS2	0.06	0.31	99°	1.2	1.3	0.13	0.10	0.35
TS4	0.10	0.28	94°	1.2	1.4	0.13	0.08	0.31
TS5	0.06	0.28	93°	1.4	1.4	0.13	0.09	0.33
TS7	0.06	0.35	111°	1.0	1.2	0.12	0.08	0.27
TS10	0.10	0.33	106°	1.0	1.1	0.14	0.10	0.35
TSE	0.05/0.13	0.2/0.28	110°	–	–	–	–	–

If a numerical method is consistent, grid refinement by a sufficient ratio reveals the magnitude of the numerical errors and prevents serious deception. Note also that energy conservation by centered schemes degrades on non-uniform grids, and that none of the time-integration schemes in common use are energy-conserving. In the LES regions of the present simulations, the energy removal by upwinding is comparable with the removal by the SGS model. This was ascertained by varying the C_{DES} constant (defined in Appendix A), and finding a much weaker sensitivity than in our study of homogeneous turbulence with a centered scheme. We accept the fact that numerical errors are not driven to negligible levels. The principle remains that concurrent grid and time-step refinement reduces all sources of numerical error, as well as the SGS viscosity. The latter is not formally a numerical error, but we normally wish to reduce it, as long as the grid can resolve the resulting field.

The grid count is reported in the directions (θ, r, z) . The grids have three blocks, with a coarser spacing in the irrotational region, relative to the near-wall and wake regions. This is seen in Figure 1. As a result, the grid reported here as (150, 109) has only about 10,000 points.

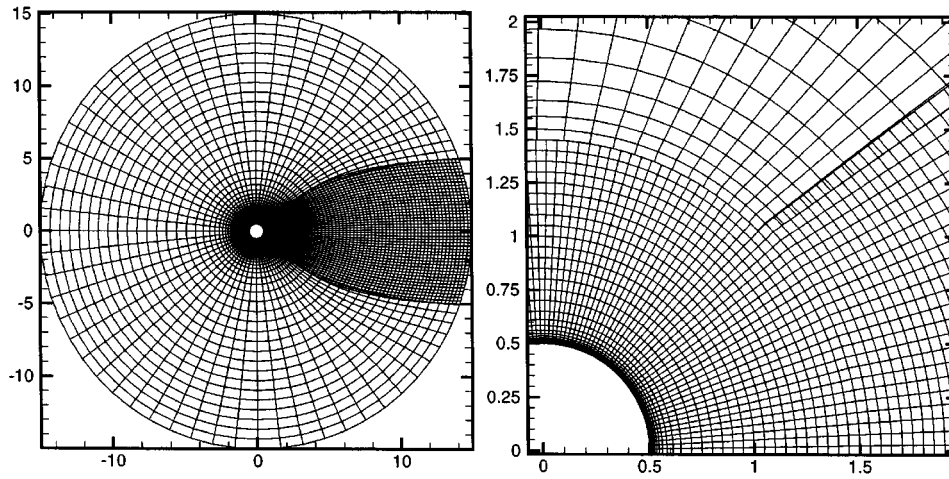


Figure 1. Medium computational grid, Case TS2. Inner block 150×36 , wake block 74×36 , outer block 59×30 . The three blocks meet near $x = 1.06$, $y = 1.03$.



Figure 2. Visualisation of Case LS5. Surfaces $\lambda_i = 1$.

Reported in Table I are the time sample t normalized with freestream velocity U_∞ and D , drag coefficient C_d , and base pressure coefficient C_{pb} . Table II continues with the lift-coefficient rms C_l' , Strouhal number St , and separation angle θ_{sep} , based on the skin friction crossing zero. L_r is the length of the recirculation bubble, from the base to the zero-mean-velocity point on the centerline, and L_{vv} is the location of the peak in $\overline{v'v'}$, relative to the back of the body. The Reynolds-stress peaks are taken in the wake, off-centerline for $\overline{u'u'}$ and $\overline{u'v'}$.

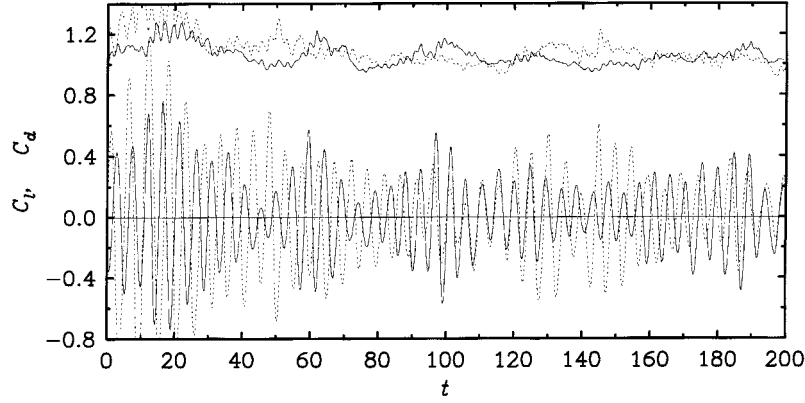


Figure 3. Time-dependent forces. Upper curves, C_d ; lower, C_l . —, LS1; - - -, LS8.

2.2. RESULTS

2.2.1. Time-Dependent Behavior

The flow visualisation in Figure 2 is meant to build confidence in the three-dimensional character of the solutions, and the domain size. The grid resolution is the medium one. We use the imaginary part λ_i of the eigenvalue of the velocity-gradient tensor, as suggested by Perry and Chong [17] to bring out vortices. The figure reveals a dominant 2D von Kármán vortex-shedding mode, but also intense vortices transverse to the von Kármán vortices. It is very consistent with DNS and LES studies of similar flows. This figure and Figure 4 below reflect how DES functions in the boundary layers: the resolved solution is smooth, with weak variations in z and t . In TS cases the resolved field has the same appearance as in these LS cases: the boundary-layer turbulence is fully modeled, and its large eddies are not represented.

Figure 3 illustrates the strong modulations of the shedding phenomenon, with a time scale of the order of 10 times the von Kármán shedding period, but not a simple beating behavior. Higher drag comes with higher lift amplitude. This is very consistent with DNS for the flat plate at 90° [13], LES for the circular and square cylinders [2, 18] and experiments [4, 7, 21]. The modulations are not as severe as for the flat plate, based on both simulation and experiment. Short-term C_d averages for the flat plate vary from 2 to 3; here, the extremes are only about 20% different. Najjar and Balachandar also report a frequency shift; the cylinder results also contain a shift, of the order of 5%. The spectra do not show any peaks away from the principal one at $St = 0.21$ and 0.22 . For both cases in the figure, an initial transient of length 20 was removed. The figure shows that removing 30 more units would have been preferable. In fact, based on the first 10 shedding cycles ($t \leq 50$), one would conclude that the two cases are permanently different. However the rest of the samples negates that impression. The phenomenon of modulations does not appear related to smooth-wall separation, since it is present for the flat

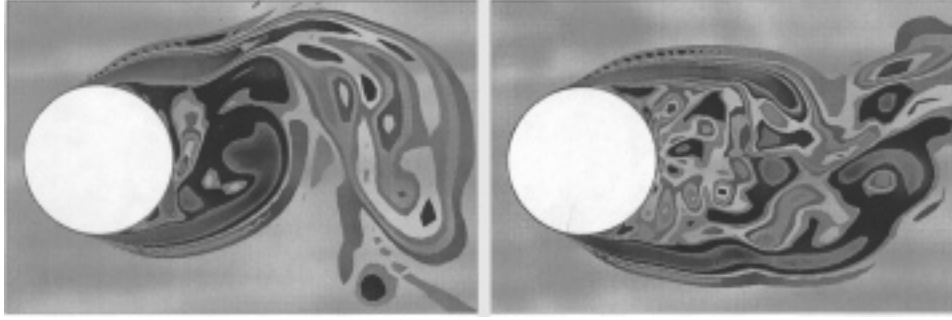


Figure 4. Vorticity contours in a plane of Case LS2. Left, at time of strong lift oscillations; right, weak oscillations.

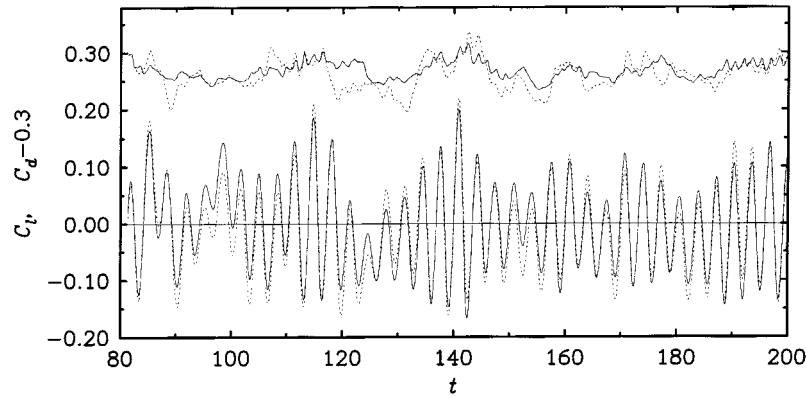


Figure 5. Time-dependent forces, case TS1. Upper curves, $C_d - 0.3$; lower, C_l . —, spanwise average; - - -, unaveraged.

plate [13]. Clearly, fine comparisons between drag coefficients, for instance, are drastically limited by this feature of the flow, particularly for the fine grids which preclude samples much beyond 100 time units on our computers. Any simulation studies that used only one or a few shedding cycles as a sample should be seriously re-examined.

Figure 4 reveals a marked visual difference between a time of high lift oscillations and one of low oscillations. These two frames are from one simulation, which is ostensibly mature in both cases: $t = 99$ and $t = 133$. Yet, a first scan of the figures would suggest that they have different grids or turbulence models. The change in flow pattern is quite similar to that described by Najjar and Balachandar [13]. On the other hand we doubt very much that it is related to that found experimentally by Norberg [16, §3.4] and attributed to the effect of finite end plates.

Figure 5 compares the forces averaged over the span $2 \times D$ of the domain and the forces on a particular section of the cylinder (one z value), as a diagnostic of the spanwise coherence. This figure illustrates, incidentally, that the modulations are nearly as pronounced in TS flows as in LS flows. However, note the different

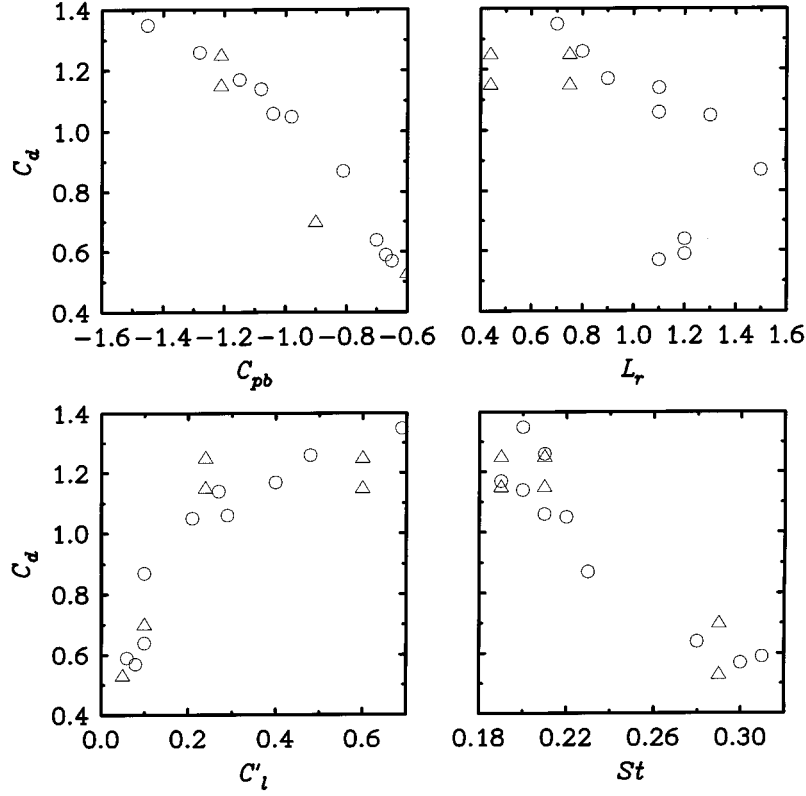


Figure 6. Correlation between global results, LS and TS cases. \circ , CFD; \triangle , Exp.

scales from those in Figure 3. The lift flatness factor $\overline{C_l^4}/(\overline{C_l^2})^2$ is 2.1 here for TS1, but 2.6 for LS1 (recall that a high flatness factor reveals irregular signals with large excursions, and that a sine wave gives a flatness equal to 1.5). The averaged and unaveraged lift signals have a very high correlation coefficient: 0.95. The rms is barely lower for the averaged lift than for the section lift: 0.077 *versus* 0.080. The conclusion is that the three-dimensionality is not coherent enough to drive the section lift ($z = 0$) until it differs much from the averaged lift ($0 \leq z < 2D$). Pointwise measurements could display larger differences. We conclude that in the range up to a few diameters, the spanwise domain size controls the lift rms less than we feared, and so comparisons between studies with somewhat different domain sizes are meaningful not only for the drag, but also for the lift.

2.2.2. Average Wall Quantities

Figure 6 displays the strong correlation between the major statistical results. LS points are clustered high in the figures (C_d always being the vertical axis) and have much variability, while TS points are low, and have less variability. We offer no hypothesis for why this is. TS cases have a larger effective statistical sample since

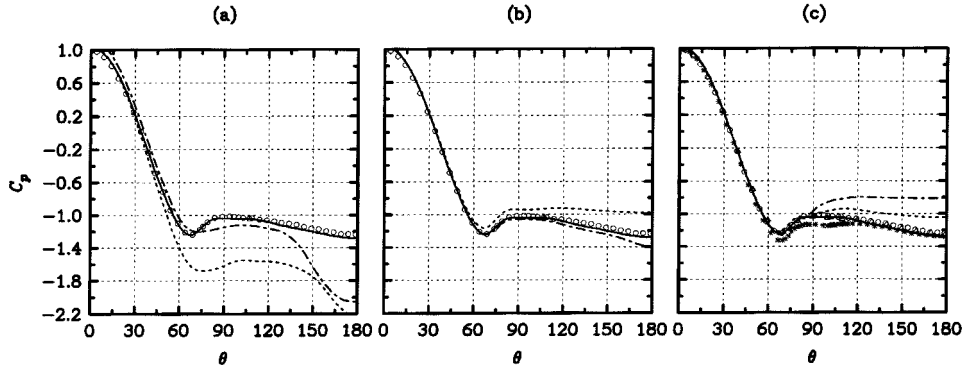


Figure 7. Pressure coefficient, LS cases. (a, b, c) \circ , Exp., $Re = 6 \times 10^4$ [15] (a) treatments, $Re = 5 \times 10^4$; —, LS2 (3D DES); - - -, LSA (2D URANS); - · - ·, L2D (2D DES). (b) grids, $Re = 5 \times 10^4$; - - -, LS1 (coarse); —, LS2 (medium); - · - ·, LS3 (fine). (c) Reynolds number; —, LS2 $Re = 5 \times 10^4$; - - -, LS8 $Re = 1.4 \times 10^5$ medium grid; - · - ·, LS7 $Re = 1.4 \times 10^5$ coarse grid; \triangle , Exp., $Re = 1.4 \times 10^5$ [4]; *, Exp., $Re = 2 \times 10^5$ [15].

their frequency is higher, but not enough to make such a difference. The LS7 case nearly bridges the LS and TS series, and will be discussed shortly.

Of course, the correlation between C_d and C_{pb} is nearly trivial. That between C_d and L_r is also unmistakable and in the same direction as for the flat plate [13], but unlike the one with C'_l and St it does not appear to plausibly place LS and TS flows on the same curve. Drag is correlated with shedding frequency (also apparent in Figure 3, where it can be seen by measuring the period of the lift coefficient during low- and high-drag conditions), in the expected direction: lower frequency for a wider wake. Finally, the correlation between C_d and C'_l (which is evident both between cases and in time, see Figure 3) is non-trivial and instructive. However, Figure 6 probably represents a failure to obtain unique results even using samples which appear very long. Table I shows that C'_l is *not* correlated with numerical or model parameters, except within the LS1–LS3 series.

We conjecture that our system of equations has an attractor with chaotic properties. Roughly, the attractor appears to be entered in about 20 time units, or 4 shedding cycles, but an even coverage of it requires on the order of 200 time units, based on Figure 3. Even this figure of 200 may be an under-estimate. Schewe showed flow régimes sustained for over 100 time units, as did Breuer [2] with LES. The outlying point at $C'_l = 0.66$ in Figure 6 is LS3, with a sample of 186 time units.

Figure 7 compares LS pressure distributions and the subcritical experiments [4, 15]. The pressure coefficient slightly exceeds 1 at the stagnation point. This error decreases as the grid is extended to larger radii, while the base pressure is insensitive. We estimate that with an infinite domain the drag coefficient would be about 0.02 lower than the present values, obtained with a grid to $15 \times D$. Full DES performs much better than either 2D URANS and 2D DES (Figure 7a).

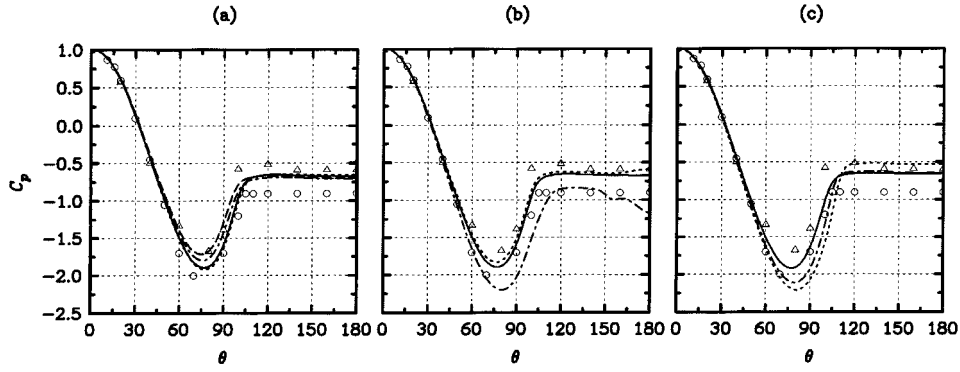


Figure 8. Pressure coefficient, TS cases. \circ , Exp., $Re = 8.5 \times 10^6$ [19]; \triangle , Exp., $Re = 7.6 \times 10^6$ [20]. (a) grid and model; - - -, TS1; —, TS2; - — -, TS4; - - -, TS5. (b) treatment; —, 3D DES (TS2); - - -, 2D URANS; —, 2D DES. (c) Reynolds number and model; —, TS2; - - -, TS7; - — -, TS10.

Two-dimensional simulations give too much drag [11, 14, 22, 23]. The difference between DES cases is tangible; in other words, grid convergence is not achieved for LS cases. This is consistent with the findings of Breuer [3], who used finer grids than even our fine one, at $Re = 140,000$. The trend in Figure 7b is smooth and monotonic from coarse through medium to fine grid, suggesting that sampling errors are minor. Unfortunately, while the medium-grid results are very close to the experiment, the fine-grid results move away from it. Similar simulations [8, 12] also reveal drifts in the drag coefficient, for instance, and some of the time samples used in these studies are clearly too short. The Reynolds-number test in Figure 7c also brings a disappointment in the sense that the base pressure is sharply increased, in contrast with the experimental trend which is a slight decrease. Flow visualizations reveal vortex roll-up in the shear layer shortly after separation, leading to a much increased pressure recovery, which is premature for a smooth cylinder at $Re = 1.4 \times 10^5$. This may be described as under-resolved transition. The phenomenon is weaker on the medium grid, LS8, than on the coarse LS7 which appears blatantly under-resolved. Unfortunately the fine-grid case LS9 is not available, and there is no proof that a grid finer than LS9 will not be needed. Such a grid would approach DNS over the crucial region of the flow, which is the extreme limiting behavior of DES.

In Figure 8 the TS results are from two grids, two models and three turbulence treatments at Reynolds number 1.4×10^5 and 3×10^6 . The TS situation would be obtained in an experiment by tripping the boundary layer well ahead of separation, but here we compare with untripped experiments at very high Reynolds numbers. We assumed that transition would be complete in the boundary layers long before separation. In Figure 8 the disagreement between experiments is tangible, in terms of crest and base pressure although not much in terms of apparent separation location. DES results fall between experiments, and the TS cases give much less

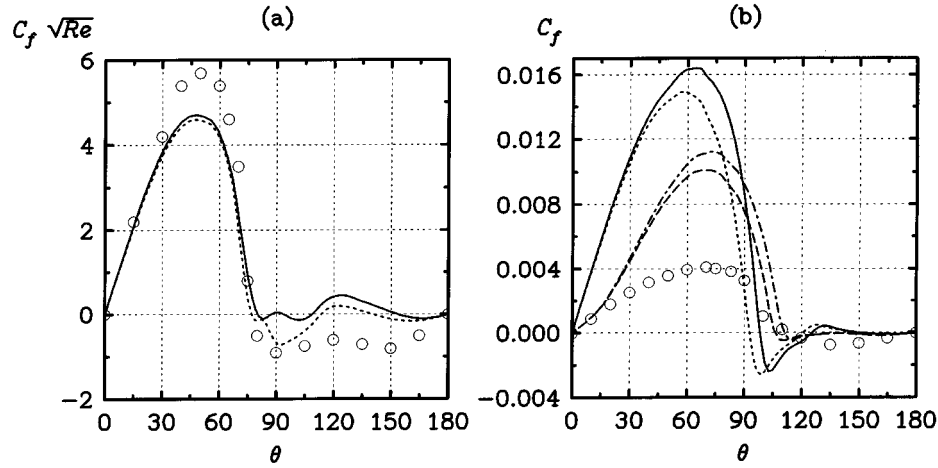


Figure 9. Skin-friction coefficient. (a) LS cases; —, LS2, $Re = 5 \times 10^4$; - - -, LS8, $Re = 1.4 \times 10^5$; \circ , Exp., $Re = 1 \times 10^5$ [1]. (b) TS cases; —, TS2; - - -, TS5; - · - ·, TS7; - - - -, TS10; \circ , Exp., $Re = 3.6 \times 10^6$ [1].

concern over grid effects than the LS cases. A turbulent separating layer is less grid-sensitive than one that is on the verge of transition.

Figure 8b shows that in a TS case, URANS results are very close to DES results. The 2D DES is also closer to full DES here than in the LS flow. A likely reason is that the TS flow has much weaker shedding and a narrower wake, which reduces the role of the largest eddies in setting the Reynolds stresses. Figure 8c shows Cases TS7 and TS10, with a high Reynolds number. The grids are coarse and the samples not very long, but the results are smooth. Separation occurs noticeably too late in TS7, putting the base pressure somewhat outside the experimental bracket, and the drag coefficient clearly outside the bracket. This is greatly improved by the curvature term in the turbulence model for TS10.

We turn to skin friction. Figure 9a reveals a fair agreement for LS cases, using the scaling by \sqrt{Re} as appropriate for laminar boundary layers. We use Achenbach's skin friction, the only one available, even though we omitted his pressures from other figures [1]. These pressures are consistently lower than in the majority of experiments, implying a higher edge velocity for the boundary layer and therefore a higher skin friction, by roughly 10%. Figure 9a is consistent with this effect, but the differences are near 20%. After separation, all datasets give low values, but the agreement is rather poor, even qualitatively. Statistical noise is evident in the simulations.

Figure 9b displays drastic differences between simulation and experiment for the skin friction in TS mode. The simulations are fully turbulent and produce typical C_f levels based on boundary-layer edge velocity, but it is clear that Achenbach's experiment had laminar boundary layers up to near the separation line even though we took his highest Reynolds number. It is a signal that fully turbulent sim-

ulations are *not* the definitive approach even at Reynolds numbers in the millions. With $Re = 1.4 \times 10^5$ in TS2 and TS5, the eddy viscosity is in fact low under the favorable pressure gradient especially with the RC term, and the skin friction is essentially the same as in laminar flow: $C_f \sqrt{Re}$ peaks at 5.6, which compares closely with Figure 9a once we recall the higher edge velocities in TS flows. This is consistent with our experience that tripping the boundary layer somewhere in the favorable gradient instead of growing eddy viscosity from the stagnation point does not affect separation much at all [22]. The high-Reynolds-number TS7 and TS10 cases have interesting features. First, the initial C_f rise for $\theta \leq 15^\circ$ is close to the laminar level. Second, the skin friction is very weak after separation, as in the experiment. Third, separation is late in TS7, which indicates that the RC term is more beneficial at this Reynolds number than at lower ones. The ratio of boundary-layer thickness δ to the radius of curvature is 0.013, so that a very noticeable effect was to be expected on the turbulence level and skin friction.

Figure 9b leaves us with a serious concern over the transition/ separation physics, in the sense that transition may never be complete upstream of separation. It is not simple to decipher the experimental C_f distributions, which are time-averaged. Achenbach's at $Re = 8.5 \times 10^5$ has a narrow peak that evidently reveals transition, but curiously the peak is absent at 3.6×10^6 . Roshko shows a pressure distribution by Flachsbart at $Re = 6.7 \times 10^5$, with a clear flat spot as with a separation bubble. Presumably, the much weaker shedding amplitudes at that Reynolds number allowed the feature to show through the time averaging. See also Cantwell's result at 1.95×10^5 (not shown here). Normally, the sequence of laminar separation and turbulent reattachment is within the reach of RANS models, functioning in tripless mode as in our LS cases here [28]. However, it may require a finer grid than is practical for a complete geometry.

2.2.3. Statistics in the Wake

Figure 10 contains velocity profiles and contours. The agreement with experiment [4] is poor, particularly on the coarser grid, as the mean recirculation bubble closes much farther downstream. Its length L_r also displays rather wide variations in the table, correlated with the lift rms, C'_l and the drag coefficient C_d as mentioned in the context of Figures 3 and 6. Breuer [3] also had tangible variations, and it appears that wake statistics are far from converged in simulations, whether DES, LES or probably even DNS. It is not simple to attribute these difficulties between spatial, temporal, domain-size and sampling errors. Our results would agree better with experiments at lower Reynolds numbers [18]. This might be a consequence of weak mixing, due to a lack of resolution. In our grid design, we gave the wake beyond one diameter a low priority.

Figure 11 shows qualitative agreement with experiment [4] for the Reynolds stresses in the wake, but the quantitative disagreements are very tangible in the roll-up region, for $x < 2.5$. The agreement is considerably better near $x = 4$, for reasons unknown. We observe smaller differences between our cases than Breuer

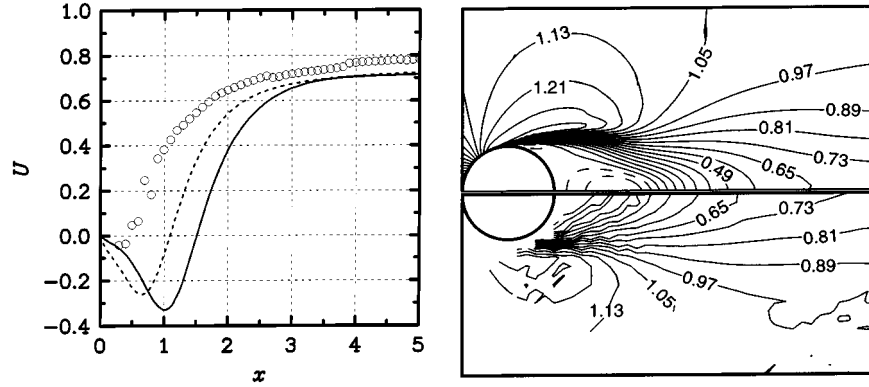


Figure 10. Centerline velocity U_{cl} , $Re = 1.4 \times 10^5$. Left, lines; \circ , Exp. [4]; —, LS7; - - -, LS8. Right, contours; Upper, LS8; lower, Exp. [4].

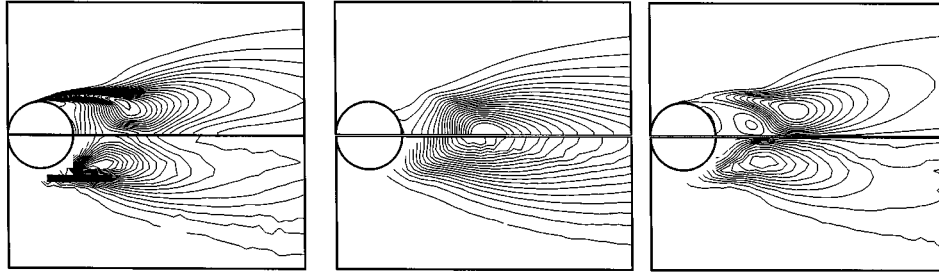


Figure 11. Reynolds stresses $\overline{u'u'}$, $\overline{v'v'}$ and $\overline{u'v'}$. Upper, LS8; lower, Exp. [4]. Contour intervals 0.0125, 0.0126, and 0.022.

did between his. Peak values are given in Table II. Our values exceed the measurements, as well as most previous LES results [8]. The low Reynolds number of the LES, namely less than 6,000, contributes to this, but the experiment was at 140,000. It is also curious that our higher stresses would allow a *longer* recirculation bubble than in the experiment, and also that the location of the peak $\overline{v'v'}$ agrees quite well, when the bubble length does not (Table II). It is tempting to challenge the experimental value of L_r , but it would be unusual to place a higher confidence in Reynolds-stress measurements than in mean-flow measurements, especially in view of the emphasis on the flying-probe technique. Note also that Cases LS2 and LS3 are much closer to experiment for L_r , but much farther for the stress levels. They follow the expected trend, that more intense turbulence makes the bubble shorter.

3. Outlook

This study of the circular cylinder with laminar and with turbulent separation and Reynolds numbers up to 3×10^6 , using Detached-Eddy Simulation, met with partial

success. The upper limit for complete success today appears to be a Reynolds number of a few thousand [11, 18], and these simulations are essentially direct simulations. We place hopes in further efforts with finer grids and lower numerical dissipation, but numerical quality alone will not resolve the transition issues. Our treatment of transition could be described as simplistic, considering the subtleties of the circular cylinder; we could expect to reproduce the gross effect of the drag crisis, and we did. The principal lessons concern the logistics of simulations for chaotic systems, the transition issues, and the DES technique.

Regarding chaotic behavior, it is satisfying for simulations to reproduce that feature of the experiment. It is another element of confidence. Unfortunately the logistical consequences are heavy. The length of time samples needed to firm up a drag coefficient to much less than 5% is considerable. This makes rigorous comparisons between methods, grids, or turbulence models dubious, once a good accuracy level has been reached [3]. The rather disturbing scatter in experiments further damages the level of focus that is achievable especially in the TS range, and we must always be alert for compensating errors.

Regarding transition, many challenges remain. We planned on avoiding the critical boundary-layer states and entered the study with the assumption that at postcritical Reynolds numbers ($Re \geq 3 \times 10^6$) the boundary layers were turbulent well ahead of separation, leading to a relatively simple modeling problem (equivalent to tripping the flow in an experiment). This assumption is negated by skin-friction measurements, and in fact our own post-processing transition calculations (not shown). Fortunately, this does not appear to displace the separation point much. However, the Reynolds-number range from 10^5 to 3×10^6 is too wide to ignore, and we are planning an effort in that range. A striking outcome would be to observe unprovoked asymmetric states (but preliminary runs with the boundary layer tripped on one side only give a rather low lift coefficient, $C_l \approx 0.35$). We can only hope that the sensitive Reynolds-number range is narrower in practical applications.

Regarding DES, the fair stability of the results under grid, model, and Reynolds-number changes is a favorable finding, although the $Re = 140,000$ case demands much further study. The ability to sustain three-dimensionality in a 2D geometry is confirmed, and the shedding frequencies are very good. While the agreement with experiment is not perfect, major features of separated flows such as the level pressure on the back of the cylinder are correct with DES, and not with URANS. On the other hand, we are unable to demonstrate “grid convergence” even with a factor of 2 change in all directions. For us as for Breuer [3], the rewards of grid refinement are uncertain. We are running a complex numerical-physical system with numerous sources of error, especially in TS cases; when these compensate, the reduction of one error does not drive the solution towards perfection. Perfection could not even be recognized, since it is not achieved in experiments.

Appendix A: Background on DES

A.1. DEFINITION OF THE TECHNIQUE

A Detached-Eddy Simulation is a three-dimensional unsteady numerical solution using a single turbulence model, which functions as a sub-grid-scale model in regions where the grid density is fine enough for a large-eddy simulation, and as a Reynolds-averaged model in regions where it is not. Essentially, SGS function or “LES mode” prevails where the grid spacing in all directions is much smaller than the thickness of the turbulent layer. The model senses the grid density and adjusts itself to a lower level of mixing, relative to “RANS mode”, in order to unlock the larger-scale instabilities of the flow and to let the energy cascade extend to length scales close to the grid spacing. In other regions, primarily boundary layers, the model is in RANS mode (however the computed solution is generally unsteady also in this region). There is a single velocity and model field, and no issue of smoothness between regions.

A formulation based on the one-equation S-A model is the following [26]. The standard RANS model uses the distance to the closest wall, d , as a length scale [25]. The DES modification consists in substituting for d , everywhere in the equations, the new length scale \tilde{d} . This length depends on the grid spacing Δ :

$$\tilde{d} \equiv \min(d, C_{\text{DES}}\Delta),$$

where Δ is based on the largest dimension of the grid cell:

$$\Delta \equiv \max(\Delta x, \Delta y, \Delta z).$$

Here we have assumed for ease that the grid is structured and that the coordinates (x, y, z) are aligned with the grid cell, but the generalization is obvious. Since the adjustment of C_{DES} matters most when the cells are nearly cubic, a general definition covering unstructured grids is to take for Δ the diameter of the grid cell, divided by $\sqrt{3}$.

The empirical constant C_{DES} was calibrated to 0.65, and is not very critical [23].

A.2. RAISON D’ÊTRE OF DES

DES is a response to two considerations which arise in the treatment of turbulence at the Reynolds numbers encountered in transportation [26]. The first is that the cost of LES in the entire boundary layer, if turbulent, exceeds our computing power by orders of magnitude. This would be true even if the problem of “wall modeling” in LES were to be solved so that, in contrast to most LES methods today, the grid spacing became unlimited in wall units. Therefore, RANS is the only choice for most of the boundary layer.

The second consideration is less clear cut, but also critical. The flow past vehicles and airplane components such as the landing gear causes massive three-dimensional separation. The hope that RANS turbulence models will soon achieve

engineering accuracy in these regions is not supported by their rate of progress over the last twenty years, even at the highest complexity level (full Reynolds-stress transport), and even with the benefit of unsteady solutions. Reynolds averaging may create an unsurmountable problem when the dominant eddies are highly geometry-specific, in contrast with the fairly “standard” eddies found in the few thin shear flows used to calibrate models. Some structural and noise applications also require unsteady flow information (including frequencies higher than those allowed by unsteady RANS). Therefore, LES is an attractive choice for the separated regions.

Let us denote by L the overall size of the flow, and l the local size of the energetic eddies. In LES the grid spacing needs to scale with l , at the largest, in fact a buffer of eddy sizes that are less geometry-specific is needed for an accurate simulation. Although eddies which have escaped from the wall in a separated region, or “detached eddies”, satisfy the relationship $l \ll L$, they still create a manageable computing problem, say of the order of 64^3 grid points. In contrast, the boundary layer imposes $l \ll \delta \ll L$, which is considerably more severe once the four dimensions are taken into account.

A DES solution has regions in which $\tilde{d} = d$, and the model functions as a RANS model. These correspond to boundary-layer type grids, which have $\Delta \gg \delta \geq d$. The solution also has regions in which $\tilde{d} = C_{\text{DES}}\Delta$, and the model functions as a subgrid-scale (SGS) model. This is seen from dimensional analysis, and was verified in homogeneous turbulence: for a given dissipation rate the eddy viscosity scales with $\Delta^{4/3}$, and indeed allows the energy cascade down to a length scale proportional to Δ . *The two regions are not explicitly distinguished, or coupled; there is a single velocity and eddy-viscosity field.* The same equations are solved, it is only that \tilde{d} is on the d or the $C_{\text{DES}}\Delta$ branch. The behavior of the model is controlled by the user, when designing the grid. Relative to unsteady RANS, the change of formulation is very minor; however, the DES poses a much heavier challenge to the numerical accuracy, in space and time.

The region in which d and $C_{\text{DES}}\Delta$ are of the same order, called “grey area”, needs much further exploration and is discussed in Section 1.

A.3. REMARKS

A.3.1. Length Scales

The formulation in Section A.1 compares the grid spacing Δ with the wall distance d , not the thickness δ of the turbulent layer (either free shear layer or boundary layer) as declared earlier in Section A.1. This is not inconsistent, because the terms that depend on \tilde{d} are the viscous and destruction terms. As a result, if a shear layer is thin compared with both the wall distance and the grid spacing, we have $\delta \ll d$ and $\delta \ll \Delta$, and the terms in question vanish. The model then is in RANS mode (i.e., insensitive to Δ). This can happen only if the grid is anisotropic and aligned

with the thin shear layer. If the grid is refined or the layer thickens sufficiently, the balance becomes $\delta \geq \Delta$, and the model switches to SGS mode.

A.3.2. *Filters*

In DES the filter is not quantitatively given. It is only known to be of the order of Δ . As a result, a set of “filtered equations” is not available, and systematic tests such as by filtering a DNS field are not possible at this stage. In our opinion, the practical benefit derived from such tests remains debatable.

A.3.3. *Choice of Base RANS Model*

DES is presented here as based on the S-A model. This model, and Secundov’s models [6], offer the most convenient length scale to inject Δ and turn a RANS model into an SGS model. However, the DES/S-A link is not fundamental, and we have started work with the SST model.

A.3.4. *Relationship to Wall-Model LES*

Many large-eddy simulations with wall modeling have used treatments that borrow from RANS models, notably the mixing-length equation and the van-Driest damping. *DES goes beyond this, in that the model in RANS mode is capable of treating an entire boundary layer or free shear layer.* This is essential to make the calculation of aerodynamic flows affordable.

A.3.5. *Separation Accuracy*

In DES, the turbulence is treated by RANS in the boundary layer and slightly beyond separation. Therefore, the need for accuracy in RANS mode is no less in DES than it is in pure RANS. An example would be the challenge posed by the maximum lift of a wing. As a result, DES models will emphasize the RANS accuracy over the SGS accuracy (most likely, they will be derived from RANS models). This is acceptable, since LES is weakly sensitive to its SGS model.

A.3.6. *Unsteady RANS Simulations*

Unsteady simulations with unmodified RANS models in some cases also enable instabilities, such as the vortex shedding past a bluff body. The difference, relative to DES, is that grid refinement does not extend the energy cascade. The solution converges to the smooth solution of the modeled equations, instead of generating smaller and smaller eddies. Typically, both the three-dimensionality and the shedding modulations are suppressed by the smoothing effect of the model, and these simulations do not have as large a potential as DES [24].

Acknowledgements

The first three authors were supported by the Boeing Technology Research Center in Moscow, and the third partly by the Russian Basic Research Foundation, grant No. 97-02-16492. We are grateful for the insight of Professors B. Cantwell and K. Squires, and Drs. J. Crouch, L. Hedges, L. Ng, and C. Norberg, and for numerous specific comments from the reviewers.

References

1. Achenbach, E., Distribution of local pressure and skin friction around a circular cylinder in cross-flow up to $Re = 5 \times 10^6$. *J. Fluid Mech.* **34**(4) (1968) 625–639.
2. Breuer, M., Large eddy simulation of the subcritical flow past a circular cylinder: Numerical and modeling aspects. *Internat. J. Numer. Methods Fluids* **28** (1998) 1281–1302.
3. Breuer, M., A challenging test case for large eddy simulation: high Reynolds number circular cylinder flow. In: Banerjee, S. and Eaton, J.K. (eds), *1st International Symposium on Turbulent Shear Flow Phenomena I*, Santa Barbara, U.S.A., September 12–15. University of California (1999) pp. 735–740. Also to appear in *Internat. J. Heat Fluid Flow* (2000).
4. Cantwell, B. and Coles, D., An experimental study of entrainment and transport in the turbulent near wake of a circular cylinder. *J. Fluid Mech.* **136** (1983) 321–374.
5. Constantinescu, G. and Squires, K.D., LES and DES investigations of turbulent flow over a sphere. AIAA 2000-0540 (2000).
6. Gulyaev, A.N., Kozlov, V.Ye. and Secundov, A.N., A universal one-equation model for turbulent viscosity. *Fluid Dynam.* **28**(4) (1993) 485–494 [translated from Russian, Consultants Bureau, New York].
7. Humphreys, J.S., On a circular cylinder in a steady wind at transition Reynolds numbers. *J. Fluid Mech.* **9** (1960) 603–612.
8. Jordan, S.A. and Ragab, S.A., A large-eddy simulation of the near wake of a circular cylinder. *J. Fluids Engrg.* **120** (1998) 243–252.
9. Karniadakis, G.E. and Triantafyllou, G.S., Three-dimensional dynamics and transition to turbulence in the wake of bluff objects. *J. Fluid Mech.* **238** (1992) 1–30.
10. Kim, J., Moin, P. and Moser, R.D., Turbulence statistics in fully developed turbulent channel flow at low Reynolds number. *J. Fluid Mech.* **177** (1987) 133.
11. Kravchenko, A.G. and Moin, P., Numerical studies of flow over a circular cylinder at $Re_D = 3900$. *Phys. Fluids* **12**(2) (2000) 403–417.
12. Mittal, R. and Balachandar, S., Effect of three-dimensionality on the lift and drag of nominally two-dimensional cylinders. *Phys. Fluids* **7**(8) (1995) 1841–1865.
13. Najjar, F.M. and Balachandar, S., Low-frequency unsteadiness in the wake of a normal flat plate. *J. Fluid Mech.* **370** (1998) 101–147.
14. Najjar, F.M. and Vanka, S.P., Effects of intrinsic three-dimensionality on the drag characteristics of a normal flat plate. *Phys. Fluids* **7**(10) (1995) 2516–2518.
15. Norberg, C., Pressure forces on a circular cylinder. In: Eckelmann, H. et al. (eds), *Bluff-Body Wakes, Dynamics and Instabilities*. Springer-Verlag, Berlin (1993) pp. 275–278.
16. Norberg, C., An experimental investigation of the flow around a circular cylinder: Influence of aspect ratio. *J. Fluid Mech.* **258** (1994) 258–287.
17. Perry, A.E. and Chong, M.S., A study of eddying motions and flow patterns using critical point concepts. *Ann. Rev. Fluid Mech.* **19** (1987) 125.
18. Rodi, W., Large-eddy simulations of the flow past bluff bodies. In: Launder, B.E. and Sandham, N.H. (eds), *Closure Strategies for Turbulent and Transitional Flows*. Cambridge University Press, Cambridge (2000) to appear.

19. Roshko, A., Experiments on the flow past a circular cylinder at very high Reynolds number. *J. Fluid Mech.* **10**(3) (1961) 345–356.
20. van Nunen, J.W.G., Pressure and forces on a circular cylinder in a cross flow at high Reynolds numbers. In: Naudascher, E. (ed.), *Flow Induced Structural Vibrations*. Springer-Verlag, Berlin (1974) pp. 748–754.
21. Schewe, G., On the force oscillations acting on a circular cylinder in crossflow from subcritical up to transcritical Reynolds numbers. *J. Fluid Mech.* **133** (1983) 265–285.
22. Shur, M.L., Spalart, P.R., Strelets, M.Kh. and Travin, A.K., Navier–Stokes simulation of shedding turbulent flow past a circular cylinder and a cylinder with a backward splitter plate. In: Desideri, G.A., Hirsch, C., Le Tallec, P., Pandolfi, M. and Periaux, J. (eds), *Third ECCOMAS CFD Conference*, Paris, September. John Wiley & Sons, Chichester (1996) pp. 676–682.
23. Shur, M., Spalart, P.R., Strelets, M. and Travin, A., Detached-eddy simulation of an airfoil at high angle of attack. In: Rodi, W. and Laurence, D. (eds), *4th International Symposium on Engineering Turbulence Modelling and Measurements*, Corsica, May 24–26. Elsevier, Amsterdam (1999) pp. 669–678.
24. Spalart, P.R., Strategies for turbulence modelling and simulations. *Internat. J. Heat Fluid Flow*, to appear.
25. Spalart, P.R. and Allmaras, S.R., A one-equation turbulence model for aerodynamic flows. *La Rech. Aéronautique* **1** (1994) 5–21.
26. Spalart, P.R., Jou, W.-H., Strelets, M. and Allmaras, S.R., Comments on the feasibility of LES for wings, and on a hybrid RANS/LES approach. In: Liu, C. and Liu, Z. (eds), *Advances in DNS/LES*, Proceedings of 1st AFOSR International Conference on DNS/LES, Ruston, LA, August 4–8. Greyden Press, Columbus, OH (1997) pp. 137–147.
27. Spalart, P.R. and Shur, M., On the sensitization of simple turbulence models to rotation and curvature. *Aerosp. Sci. Techn.* **1**(5) (1997) 297–302.
28. Spalart, P.R. and Strelets, M.Kh., Mechanisms of transition and heat transfer in a separation bubble. *J. Fluid Mech.* **403** (2000) 329–349.
29. Szechenyi, E., Supercritical Reynolds number simulation for two-dimensional flow over circular cylinders. *J. Fluid Mech.* **70**(3) (1975) 529–542.
30. Szepessy, S., On the spanwise correlation of vortex shedding from a circular cylinder at high subcritical Reynolds number. *Phys. Fluids* **6**(7) (1994) 2406–2416.
31. Zdravkovich, M.M., *Flow around Circular Cylinders*. Oxford University Press, Oxford (1997).